CORROSION SCIENCE AND TECHNOLOGY, Vol.19, No.2(2020), pp.82~88
[Research Paper]
pISSN: 1598-6462 / eISSN: 2288-6524
DOI: https://doi.org/10.14773/cst.2020.19.2.82

Synthesis and Characterization of Hydrotalcite/Graphene Oxide Containing Benzoate for Corrosion Protection of Carbon Steel

Thuy Duong Nguyen[1], Boi An Tran[2], Ke Oanh Vu[1], Anh Son Nguyen[1], Anh Truc Trinh[1], Gia Vu Pham[1], Thi Xuan Hang To[1,3,†], and Thanh Thao Phan[2]

[1]*Institute for Tropical Technology, Vietnam Academy of Science and Technology, 18 Hoang Quoc Viet, Cau Giay, Hanoi, Vietnam*
[2]*Institute of Chemical Technology, Vietnam Academy of Science and Technology, 1 Mac Dinh Chi, District 1, Ho Chi Minh, Vietnam*
[3]*Graduate University of Science and Technology, Vietnam Academy of Science and Technology, 18 Hoang Quoc Viet, Cau Giay, Hanoi, Vietnam*

(Received February 28, 2020; Revised March 30, 2020; Accepted March 30, 2020)

This work examined the corrosion protection performance of benzoate loaded hydrotalcite/graphene oxide (HT/GO-BZ) for carbon steel. HT/GO-BZ was fabricated by the co-precipitation method and characterized by infrared spectroscopy, X-ray diffraction, and scanning electronic microscopy. The corrosion inhibition action of HT/GO-BZ on carbon steel in 0.1 M NaCl solution was evaluated by electrochemical measurements. The benzoate content in HT/GO-BZ was determined by UV-Vis spectroscopy. Subsequently, the effect of HT/GO-BZ on the corrosion resistance of the water-based epoxy coating was investigated by the salt spray test. The obtained results demonstrated the intercalation of benzoate and GO in the hydrotalcite structure. The benzoate content in HT/GO-BZ was about 16%. The polarization curves of the carbon steel electrode revealed anodic corrosion inhibition activity of HT/GO-BZ and the inhibition efficiency was about 95.2% at a concentration of 3g/L. The GO present in HT/GO-BZ enhanced the inhibition effect of HT-BZ. The presence of HT/GO-BZ improved the corrosion resistance of the waterborne epoxy coating.

Keywords: *Corrosion inhibition, Hydrotalcite, Benzoate, Graphene oxide, Waterborne epoxy coatings*

1. Introduction

Corrosion inhibitors play important role in organic coatings for corrosion protection of metals. Due to protection of environment a great research focused on synthesis and application of green inhibitors in organic coatings. Recently, acid organic inhibitors have been intensively studied for corrosion protection of metals [1-3]. Among them, benzoic acid and sodium benzoates have been studied as corrosion inhibitors for iron and steel in neutral media and also in alkaline media [4-6]. The inhibition mechanism of benzoate is based on the blocking of anodic sites by inhibitor molecules. Until now, the application of acid benzoic or benzoates in organic coatings is still limited due to their solubility in water. As one method to resolve this problem is intercalation of benzoate into inorganic container. Hydrotalcites with anion-exchange capability have been widely investigated as containers of corrosion inhibitors in organic coatings. Hydrotalcites intercalated with corrosion inhibitors can absorb the Cl^- anions and release inhibiting anions [7,8]. Corrosion inhibition efficiency of Zn-Al hydrotalcite containing benzoate is higher than 90% at concentration of 50 g/L for carbon steel in 3.5% NaCl solution [9]. Mg-Al hydrotalcite intercalated with benzoate has inhibition efficiency of 96% at concentration of 15 g/L for carbon steel in simulated concrete pore solution (mixture of saturated $Ca(OH)_2$ + 0.3 mol/L NaCl) [10].

Graphene oxide (GO) has been intensively investigated for corrosion protection of metals due to its excellent mechanical and barrier properties. GO coating formed by electrophoresis deposition on steel showed superior corrosion protection for steel [11]. Graphene oxide modified by P-phenylenediamine improved corrosion protection of

†Corresponding author: ttxhang60@gmail.com

epoxy coatings [12]. Surface treatment by aminosilane and 1,4-butanediol diglycidyl improved their GO dispersion in epoxy matrix and effects on corrosion resistance of epoxy coatings [13]. GO modified by 3-(triethoxysilyl) propylisocyanate and 3-aminopropyltriethoxysilane significantly improved the corrosion resistance and adhesion properties of silane/epoxy coatings on steel surface [14]. GO was grafted with polyethylenimin and applied in waterborne epoxy coating for corrosion protection of carbon steel [15].

The combination of hydrotalcite and graphene oxide has been studied for different applications such as energy storage, catalysts, adsorbents, fire retardants. Only few researches reported the application of hydrotalcite/graphene oxide materials for corrosion protection of metals. Reduced GO/hydrotalcite with the ratio of 2/1 at concentration of 0.5% improved protective properties of waterborne epoxy coating [16].

In our previous works, hydrotalcite intercalated with benzoate (HT-BZ) and hydrotalcite/graphene oxide hybrid (HT/GO) were synthesized and applied for corrosion protection of carbon steel [17,18]. The results showed that both HT-BZ and HT/GO had inhibition effect on carbon steel and improved corrosion protection and adhesion of organic coating. The presence of graphene oxide enhanced the inhibition effect of hydrotalcite. In this work, the effect of GO on corrosion inhibition of Zn-Al hydrotalcite intercalated with benzoate (HT-BZ) was studied. For this purpose, hydrotalcite/graphene oxide hybrid loaded benzoate (HT/GO-BZ) as corrosion inhibitor for carbon steel was prepared and characterized. The corrosion inhibition effect of HT/GO-BZ for carbon steel was investigated using electrochemical method and salt fog test.

2. Experimental Methods

2.1. Materials

Graphite was supplied by Sigma-Aldrich. H_2SO_4 (95-98%), $KMnO_4$, $Zn(NO_3)_2.6H_2O$, $Al(NO_3)_3.9H_2O$, and NaOH were obtained from Merck. Sodium benzoate ($C_7H_5O_2Na$) (99%) was obtained from VWR.

For preparation of the coatings, the epoxy Epikote 828 with epoxy equivalent weight of about 187 g/eq and the hardener EPIKURE 8537-WY-60 with equivalent weight of 174 g/eq were used. The epoxy resin was obtained from Hexion, Thailand and the hardener was obtained from Momentive, Thailand.

2.2. Preparation of graphene oxide

Graphene oxide (GO) was prepared by using modified Hummer method described in our previous work [18]. Graphite was expanded in supercritical CO_2 environment at 50 °C, 15 MPa. 2 g graphite and 7 g $KMnO_4$ were slowly added into 50 mL concentrated H_2SO_4 with temperature of 2 °C. Then the reaction temperature was maintained at 35 °C for 2 hours. After that 300 mL distilled water was poured into the mixture with stirring over 1 h, then 10 mL H_2O_2 was added into the mixture with stirring over 1 h. The precipitate was filtered, washed with distilled water and dried in a vacuum oven at 50 °C for 24 h.

2.3. Preparation of HT-BZ and HT/GO-BZ

Hydrotalcite intercalated with benzoate (HT-BZ) was fabricated by the co-precipitation reaction. Solution A is a salt mixture of $Zn(NO_3)_2$ and $Al(NO_3)_3$ (molar ratio of Zn^{2+}/Al^{3+} = 2/1). Solution B is a mixture of two solutions: benzoate solution and sodium hydroxide solution. Solution B was kept under nitrogen atmosphere at room temperature and pH = 8 – 9. Solution A was added to solution B with vigorous stirring. Then slurry was kept at 50 °C for 24 h under nitrogen atmosphere. The white precipitation formed was washed with large amounts of degassed distilled water before drying at a temperature of 70 °C for 24 h.

The HT/GO-BZ was synthesized using the same procedure described for the preparation of HT-BZ, except that solution B contained GO with GO/HT weight ratio of 1/20.

2.4. Coating preparation

Waterborne epoxy coating without inhibitor and with HT-BZ and HT/GO-BZ at concentration of 0.5 wt% were applied on carbon steel plates (150 mm × 100 mm × 2 mm). The steel plates were polished with SiC papers (400 grades) and cleaned with ethanol. For preparation of epoxy coatings, the epoxy/amine ratio was the stoichiometric ratio. HT-BZ and HT/GO-BZ were dispersed in hardener solution by magnetic stirring and sonication, and then the epoxy resin was added to the hardener solution containing HT-BZ and HT/GO-BZ. The coatings were formed on carbon steel by the spin coating method. The coatings were cured at ambient temperature for 7 days. The measured thickness of dry film was 30 ± 3 μm.

2.5. Analytical characterization

Powder X-ray diffraction (XRD) patterns of HT-BZ and HT/GO-BZ were obtained on Siemens diffractometer D5000 using CuKα radiation (λ = 0.15406 nm) at room temperature from 1° to 70° with scanning speed of 2.6°/min under air conditions.

Fourier transform infrared spectra (FT-IR) of samples

were measured on Nexus 670 Nicolet spectrometer with resolution at 32 cm^{-1} using the KBr method with transmission mode. The spectra were obtained in the region of 400 - 4000 cm^{-1}.

Field emission scanning electron microscope (FESEM) of hydrotalcite powders were operated on FESEM Hitachi S-4800 at a voltage of 5.0 kV.

UV-Vis spectroscopy was used to determine the content of benzoate in HT-BZ and HT/GO-BZ with GBC Cintra 40 spectrometer. The amount of benzoate in HT-BZ or HT/GO-BZ was determined by the following protocol: 0.01 g of HT-BZ or HT/GO-BZ was dissolved in 1.2 mL of 1 M HCl solution in 50-mL volumetric flask. Then distilled water was filled into the balance of volumetric flask. The absorbance of benzoate was monitored by UV–Vis spectrophotometer at λ_{max} = 225 nm. Based on the benzoate standard curve, the content of benzoate into the HT-BZ or HT/GO-BZ was calculated. The standard curve was obtained from a series of benzoate standard solutions.

2.6. Electrochemical measurements

Corrosion inhibition effect of hydrotalcites loaded benzoate was investigated using polarization curves and electrochemical impedance spectroscopy measurements. A three-electrode cell with a platinum auxiliary electrode, a saturated calomel reference electrode (SCE) and a working electrode with an exposed area of 1 cm^2 was used. The electrochemical measurements were performed using a VSP 300 Biologic. Testing solution was a 0.1 M NaCl solution. The concentration of hydrotalcites was 3 g/L. The impedance diagrams were recorded after 2 h immersion at the open circuit potential with a frequency range from 100 kHz to 10 mHz with sinusoidal voltage of 5 mV. The polarization curves performed with a sweep speed of 1 mV/s beginning from the corrosion potential after 2 h of immersion. Each experiment was done at least three times.

2.7. Salt spray test

Corrosion resistance of coatings was evaluated by salt spray test according to ASTM B117 using Q-FOGCCT-600 chamber. The coating samples were scribed before test. The sample surfaces after 48 h testing were evaluated. Three samples of each system were tested.

3. Results

3.1. Characterization of HT/GO-BZ

Structure and morphology of HT/GO-BZ were investigated by FT-IR, XRD and SEM. The FT-IR spectra of GO, HT-BZ and HT/GO-BZ are presented in Fig.1. The FT-IR spectrum of GO shows bands at 1406 cm^{-1} and 1717 cm^{-1} corresponding to C-O and C=O vibration. The band at 1621 cm^{-1} is attributed to C=C vibration [19]. For HT-BZ it is observed bands characteristic of Zn-O and NO^{3-} group of hydrotalcite at 426 cm^{-1} and 1385 cm^{-1} [20]. The bands at 1552 cm^{-1} and 1408 cm^{-1} are attributed to vibration of COO^- group [21]. The band at 1596 cm^{-1} is characteristic of monosubstituted aromatic ring. This result indicates the intercalation of benzoate in HT-BZ. FT-IR spectrum of HT/GO-BZ presents also characteristic bands of Zn-O and COO^- vibration at 426 cm^{-1} and 1535 cm^{-1} and 1395 cm^{-1} like HT-BZ. By comparison with HT-BZ, the bands characteristic of COO^- of HT/GO-BZ are moved to lower wavenumber and their intensity are decreased. This modification can be caused by the presence of GO in HT/GO-BZ and the BZ content in HT/GO-BZ was lower than the one of HT-BZ. These results indicate the presence of benzoate in the structure of HT/GO-BZ.

The X-ray diffraction patterns of GO, HT-BZ and HT/GO-BZ are shown in Fig. 2. The XRD pattern of GO exhibits strong characteristic peak corresponding to interlayer distance of 0.79 nm. This indicates the complete oxidation of graphite to the GO [19]. The XRD patterns of HT-BZ and HT/GO-BZ are similar and present typical peaks of hydrotalcites. In the XRD patterns of HT-BZ and HT/GO-BZ present the (003) reflections corresponding to interlayer distance of 1.59 nm and 1.96 nm respectively, which are higher than the value of hydrotalcite of 0.79 nm [22]. The higher d-spacing value of the HT-BZ and HT/GO-BZ in comparison to the value of hydrotalcite

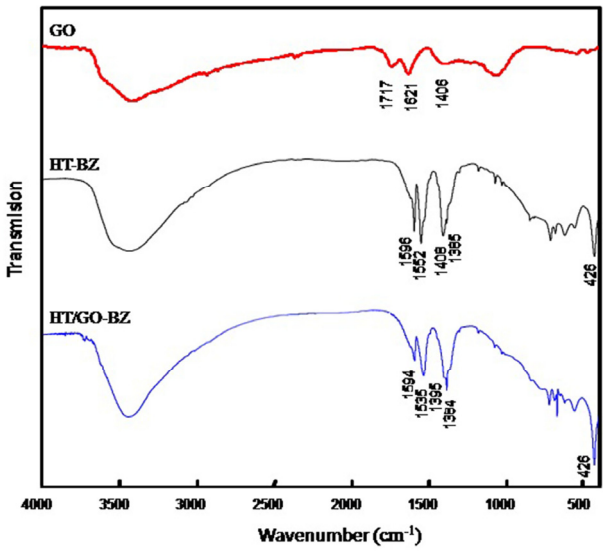

Fig. 1 FT-IR spectra of GO, HT-BZ and HT/GO-BZ.

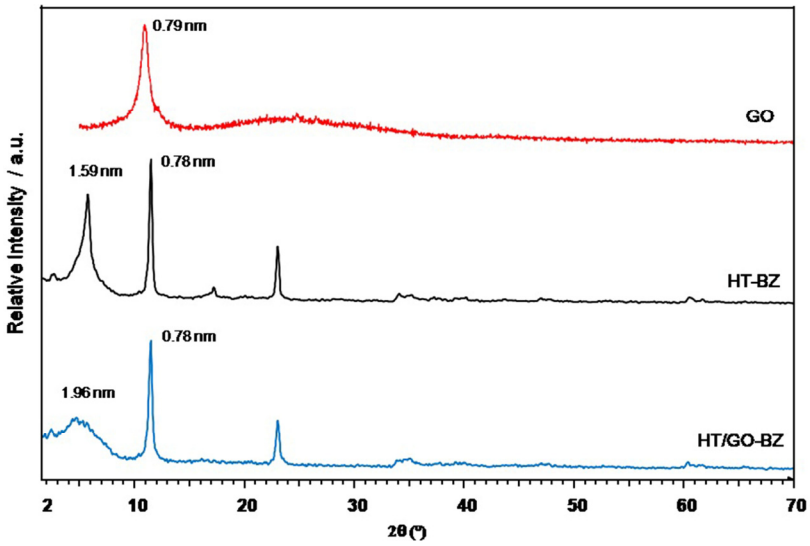

Fig. 2 XRD patterns of GO, HT-BZ and HT/GO-BZ.

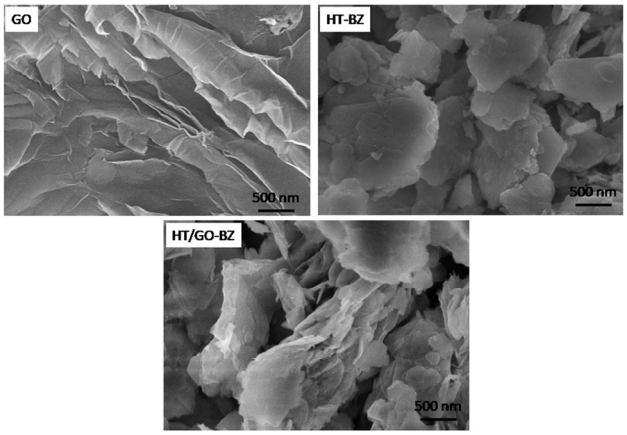

Fig. 3 SEM photographs of GO, HT-BZ and HT/GO-BZ.

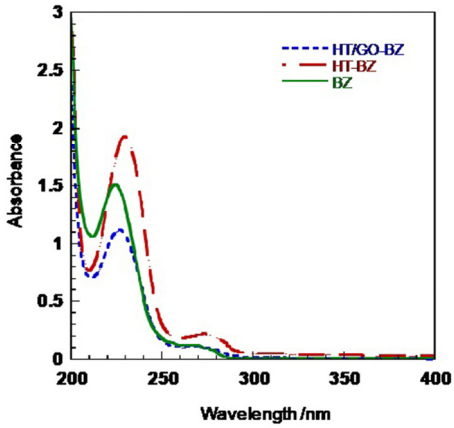

Fig. 4 UV-Vis spectra of BZ solution, solutions of HT-BZ and HT/GO-BZ after reaction with HCl.

indicates the intercalation of benzoate molecules in the interlayer domain of hydrotalcite. For HT/GO-BZ, the basal spacing is higher than this value of HT-BZ. The higher interlayer distance of HT/GO-BZ compared with the one of HT-BZ can be explained the intercalation of GO in interlayer domain of hydrotalcite. These results confirm the intercalation of benzoate and GO in the structure of HT/GO-BZ.

The SEM images of GO, HT-BZ and HT/GO-BZ are shown in Fig. 3. It can be seen that GO has layer structure with wrinkled large surface. HT-BZ presents a typical plate-like morphology of hydrotalcites and has particle size in the range of 200-500 nm. HT/GO-BZ displays also layer structure of hydrotalcites. HT/GO-BZ particles are more separated and the layer thickness is lower compared to HT-BZ. The morphology change of HT/GO-BZ compared with HT-BZ can be explained by the intercalation of GO in the interlayer domain of hydrotalcite and formation of hydrotalcites on GO surface [18,23]. The SEM result is in good agreement with XRD analysis.

The benzoate content in HT/GO-BZ was determined and compared with HT-BZ by UV-Vis spectroscopy. Fig. 4 shows the UV-Vis spectra of benzoate (BZ) solution at concentration of 1.85 10^{-4} mol/L, solution of HT-BZ and HT/GO-BZ reacted with HCl after 2 times dilution. All spectra have the max absorbance at wave length of 225 nm. The calibration curve determined from a series of benzoate standard solutions (shown in Fig. 5). The relationship between the absorbance at 225 nm and the benzoate concentration is: A = 8236 C - 0.012103 with R^2

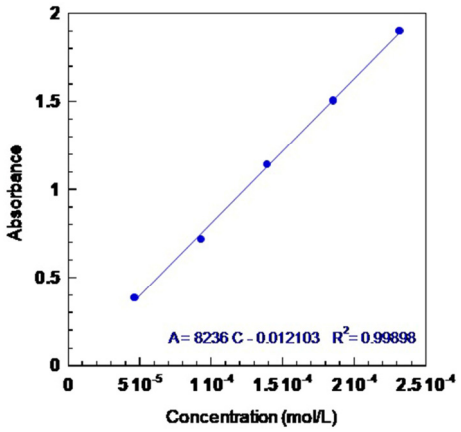

Fig. 5 Calibration curve of standard benzoate solutions.

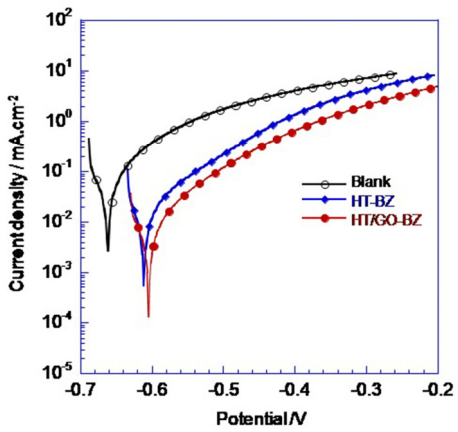

Fig. 6 Anodic polarization curves obtained for electrode after 2 h immersion in 0.1 M NaCl solution without inhibitor (○), with 3 g/L HT-BZ (◆) and with 3 g/L HT/GO-BZ (●).

= 0.99898 (C is benzoate concentration in mol/L and A is the absorbance at the wavelength of 225 nm). From the calibration curve and the absorbance at 225 nm, the benzoate concentration of the solution containing HT/GO-BZ or HT-BZ reacted with HCl was determined and then the benzoate content in HT/GO-BZ and HT-BZ was calculated. The benzoate loading in HT/GO-BZ and HT-BZ were 16% and 28% respectively. The benzoate content in HT-BZ was close to the value reported [9]. The lower benzoate content in HT/GO-BZ can be explained by the presence of GO in the interlayer of HT/GO-BZ.

3.2. Corrosion inhibition of HT/GO-BZ

Corrosion inhibition of HT/GO-BZ for carbon steel was investigated in 0.1 M NaCl solution at concentration of 3 g/L. For a comparison, the corrosion test was also realized for 0.1 M NaCl without inhibitor and with HT-BZ at 3 g/L. The anodic polarization curves and electrochemical impedance diagrams of electrodes were performed after 2 h exposure.

Fig. 6 presents the anodic polarization curves measured for steel electrode after 2 h immersion in 0.1 M NaCl solution in the absence of inhibitor and in the presence of HT-BZ and HT/GO-BZ. Corrosion potential (E_{corr}), corrosion current density (i_{corr}) determined from polarization curves are presented in Table 1. With the presence of HT-BZ and HT/GO-BZ, the corrosion potential is significantly shifted to more positive values, and the anodic current densities are lower compared to the case without inhibitor. The corrosion potential obtained for HT/GO-BZ is close to that of HT-BZ. But the anodic current densities obtained for the solution containing HT/GO-BZ are lower than the values of the solution containing HT-BZ. Benzoate released from HT-BZ and HT/GO-BZ

Table 1 Corrosion potential and corrosion current density determined for steel electrode after 2 h exposure to 0.1 M NaCl solution without inhibitor and with presence of HT-BZ and HT/GO-BZ

Sample	E_{corr} (mV)	i_{corr} ($\mu A.cm^{-2}$)
0.1 M NaCl	- 662	111
0.1 M NaCl + 3 g/L HT-BZ	- 611	28
0.1 M NaCl + 3 g/L HT/GO-BZ	- 604	14

can be adsorbed on steel surface and inhibiting the anodic corrosion reaction [6]. Although the benzoate content in HT/GO-BZ was lower than the one of HT-BZ, the anodic current densities determined for HT/GO-BZ were lower compared to HT-BZ. This behavior can be explained by the effect of GO intercalated in HT/GO-BZ. In addition, the interaction between carboxyl groups of GO intercalated in HT/GO-BZ with iron ions can improve the adsorption of HT/GO-BZ on steel surface. Besides, GO with large lateral structure and high impermeability improves the barrier properties of the film formed by HT/GO-BZ [18]. The results from polarization curves indicate that HT/GO-BZ is an anodic inhibitor of carbon steel and the presence of GO improved the inhibition effect of HT/GO-BZ.

The electrochemical impedance diagrams of steel electrodes after 2 h immersion in 0.1 M NaCl solution without inhibitor and with HT-BZ and HT/GO-BZ are shown in Fig. 7. It is observed that for all solutions, after 2 h exposure the impedance diagrams have only one time constant. The impedance modulus at low frequencies ob-

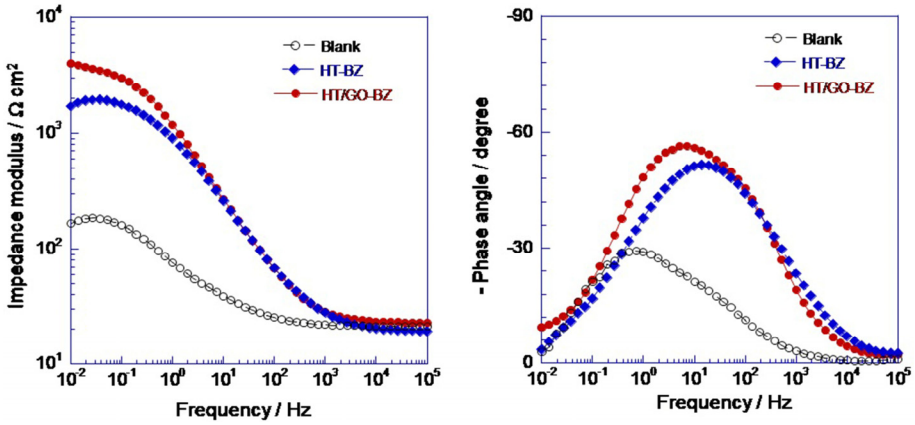

Fig. 7 Electrochemical impedance diagrams obtained for steel electrode after 2 h exposure to 0.1 M NaCl solution without inhibitor and with presence of HT-BZ and HT/GO-BZ.

Table 2 Polarization resistance and inhibition efficiencies determined for steel electrode after 2 h exposure to 0.1 M NaCl solution without inhibitor and with presence of HT-BZ and HT/GO-BZ

Sample	R_p ($\Omega.cm^2$)	Inhibition efficiency (%)
0.1 M NaCl	195	-
0.1 M NaCl + 3 g/L HT-BZ	2045	90.5
0.1 M NaCl + 3 g/L HT/GO-BZ	4070	95.2

tained for solutions containing HT-BZ and HT/GO-BZ are significantly higher than the one of blank solution. The impedance modulus for the case of HT/GO-BZ are higher than the ones for the sample with HT-BZ. From the impedance diagrams, the polarization resistances were determined and used for evaluation of inhibition efficiencies [25].

$E\% = (R_p - R_{p0})/R_p$. In this equation R_{p0} is the polarization resistance obtained for solution without inhibitor and R_p is the polarization resistance obtained for solution containing inhibitor.

The obtained R_p values and calculated inhibition efficiencies are presented in Table 2. For electrode exposed to sodium chloride solution in the absence of inhibitor, the R_{p0} is 195 $\Omega.cm^2$. The R_p value obtained in the presence of HT-BZ is 2045 $\Omega.cm^2$ and the inhibition efficiency is 90.5%. For solution containing HT/GO-BZ, the R_p value is 4070 $\Omega.cm^2$ and the inhibition efficiency is 95.2%. The results obtained from electrochemical measurements show that the presence of GO in HT/GO-BZ increased the inhibition efficiency of hydrotalcite. Higher corrosion inhibition efficiency of HT/GO-BZ compared to HT-BZ can be caused by the barrier effect of GO in HT/GO-BZ.

3.3. Corrosion resistance of water based epoxy coatings containing HT/GO-BZ

Corrosion resistance of coating system was investigated by the salt spray test. Fig. 8 presents the images of samples after 48 h test. All three samples exhibited visible corrosion and rust on the scribes. However the rust amounts at scratches of the coatings are different. It can be seen that pure epoxy coating exhibited the highest rust creep from scratch and epoxy coating loading HT/GO-BZ presented the lowest rust creep from scratch. These results show that the presence of HT-BZ and HT/GO-BZ in epoxy coating delays corrosion travels along the coating/metal interface to either sides of the scratch. Cl^- anions can be entrapped by HT-BZ and HT/GO-BZ and benzoate released can provide inhibition effect at the interface coating/metal [8,17]. The corrosion degree at scratch of sample with HT/GO-BZ was lower than that of sample with HT-BZ. This result can be explained the barrier effect of GO in HT/GO-BZ.

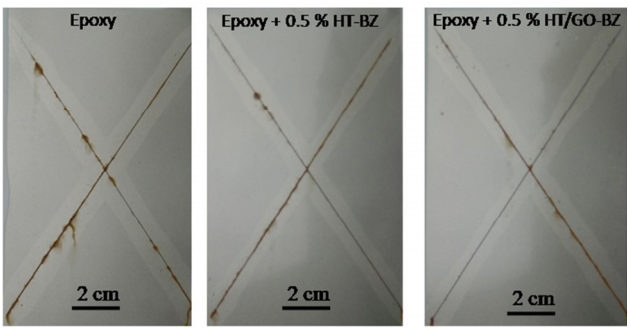

Fig. 8 Images of samples after 48 h test in salt spray chamber.

4. Conclusions

Hydrotalcite/graphene oxide containing benzoate was successfully prepared by the co-precipitation method. The benzoate content in HT/GO-BZ was about 16%. The results obtained by electrochemical measurement demonstrate that HT/GO-BZ is an anodic corrosion inhibitor with inhibition efficiency about 95.2% at 3 g/L concentration. High corrosion inhibition efficiency of HT/GO-BZ is due to the inhibition effect of benzoate and barrier effect of GO intercalated in HT/GO-BZ. Corrosion resistance of epoxy coating was increased significantly by incorporation of 0.5 wt% HT/GO-BZ.

Acknowledgments

This research is funded by Vietnam National Foundation for Science and Technology Development (NAFOSTED) under grant number 104.01-2016.06.

References

1. G. Boisier, N. Portail, and N. Pébère, *Electrochim. Acta*, **55**, 6182 (2010). https://doi.org/10.1016/j.electacta.2009.10.080
2. U. Rammelt, S. Köhler, and G. Reinhard, *Electrochim. Acta*, **53**, 6968 (2008). https://doi.org/10.1016/j.electacta.2008.01.004
3. C. Georges, E. Rocca, and P. Steinmetz, *Electrochim. Acta*, **53**, 4839 (2008). https://doi.org/10.1016/j.electacta.2008.01.073
4. U. Rammelt, S. Koehler, and G. Reinhard, *Corros. Sci.*, **50**, 1659 (2008). http://doi.org/10.1016/j.corsci.2008.02.016
5. J. Zhao and G. Chen, *Electrochim. Acta*, **69**, 247 (2012). https://doi.org/10.1016/j.electacta.2012.02.101
6. G. Blustein, J. Rodriguez, R. Romanogli, and C. F. Zinola, *Corros. Sci.*, **47**, 369 (2005). https://doi.org/10.1016/j.corsci.2004.06.009
7. S. P. V. Mahajanam and R. G. Buchheit, *Corrosion*, **64**, 230 (2008). https://doi.org/10.5006/1.3278468
8. J. Tedim, A. Kuznetsova, A. N. Salak, F. Montemor, D. Snihirova, M. Pilz, M. L. Zheludkevich, and M. G. S. Ferreira, *Corros. Sci.*, **55**, 1 (2012). https://doi.org/10.1016/j.corsci.2011.10.003
9. Y. Wang and D. Zhang, *Mater. Res. Bull.*, **46**, 1963 (2011). https://doi.org/10.1016/j.materresbull.2011.07.021
10. B. Wu, J. Zuo, B. Dong, F. Xing, and C. Luo, *Appl. Clay Sci.*, **180**, 105181 (2019). https://doi.org/10.1016/j.clay.2019.105181
11. C.-Y. Ho, S.-M. Huang, S.-T. Lee, and Y.-J. Chang, *Appl. Surf. Sci.*, **477**, 226 (2019). https://doi.org/10.1016/j.apsusc.2017.10.129
12. B. Ramezanzadeh, G. Bahlakeh, M. H. M. Moghadam, and R. Miraftab, *Chem. Eng. J.*, **335**, 737 (2018). https://doi.org/10.1016/j.cej.2017.11.019
13. M. G. Sari, M. Shamshiri, and B. Ramezanzadeh, *Corros. Sci.*, **129**, 38 (2017). https://doi.org/10.1016/j.corsci.2017.09.024
14. N. Parhizkar, B. Ramezanzadeh, and T. Shahrabi, *Appl. Surf. Sci.*, **439**, 45 (2018). https://doi.org/10.1016/j.apsusc.2017.12.240
15. F. Jiang, W. Zhao, Y. Wu, Y. Wu, G. Liu, J. Dong, and K. Zhou, *Appl. Surf. Sci.*, **479**, 963 (2019). https://doi.org/10.1016/j.apsusc.2019.02.193
16. D. Yu, S. Wen, J. Yang, J. Wang, Y. Chen, J. Luo, and Y. Wu, *Surf. Coat. Technol.*, **326A**, 207 (2017). https://doi.org/10.1016/j.surfcoat.2017.07.053
17. T. D. Nguyen, T. X. H. To, J. Gervasi, Y. Paint, M. Gonon, M.-G. Olivier, *Prog. Org. Coat.*, **124**, 256 (2018). https://doi.org/10.1016/j.porgcoat.2017.12.006
18. T. D. Nguyen, B. A. Tran, K. O. Vu, A. S. Nguyen, A. T. Trinh, G. V. Pham, T. X. H. To, M. V. Phan, and T. T. Phan, *J. Coat. Technol. Res.*, **16**, 585 (2019). https://doi.org/10.1007/s11998-018-0139-3
19. A. Esmaeili and M. H. Entezari, *J. Colloid Interf. Sci.*, **432**, 19 (2014). https://doi.org/10.1016/j.jcis.2014.06.055
20. T. D. Nguyen, T. X. H. To, A. Nicolay, Y. Paint, and M. -G. Olivier, *Prog. Org. Coat.*, **101**, 331 (2016). https://doi.org/10.1016/j.porgcoat.2016.08.021
21. P. Kovář, M. Pospíšil, M. Nocchetti, P. Čapková, and K. Melánová, *J. Mol. Model.*, **13**, 937 (2007). https://doi.org/10.1007/s00894-007-0217-4
22. T. X. H. To, A. T. Trinh, T. D. Nguyen, G. V. Pham, and H. Thai, *Appl. Clay Sci.*, **67-68**, 18 (2012). https://doi.org/10.1016/j.clay.2012.07.004
23. Y. Wang, Z. Wang, X. Wu, X. Liu, and M. Li, *Electrochim. Acta*, **192**, 196 (2016). https://doi.org/10.1016/j.electacta.2016.01.201
24. M. Outirite, M. Lagrenee, M. Lebrini, M. Traisnel, C. Jama, H. Vezin, and F. Bentiss, *Electrochim. Acta*, **55**, 1670 (2010). https://doi.org/10.1016/j.electacta.2009.10.048